Universiteit Utrecht

SRON
Netherlands Institute for Space Research

Bachelor thesis

The detection of PSR J1846-0258 at high-energy gamma-rays

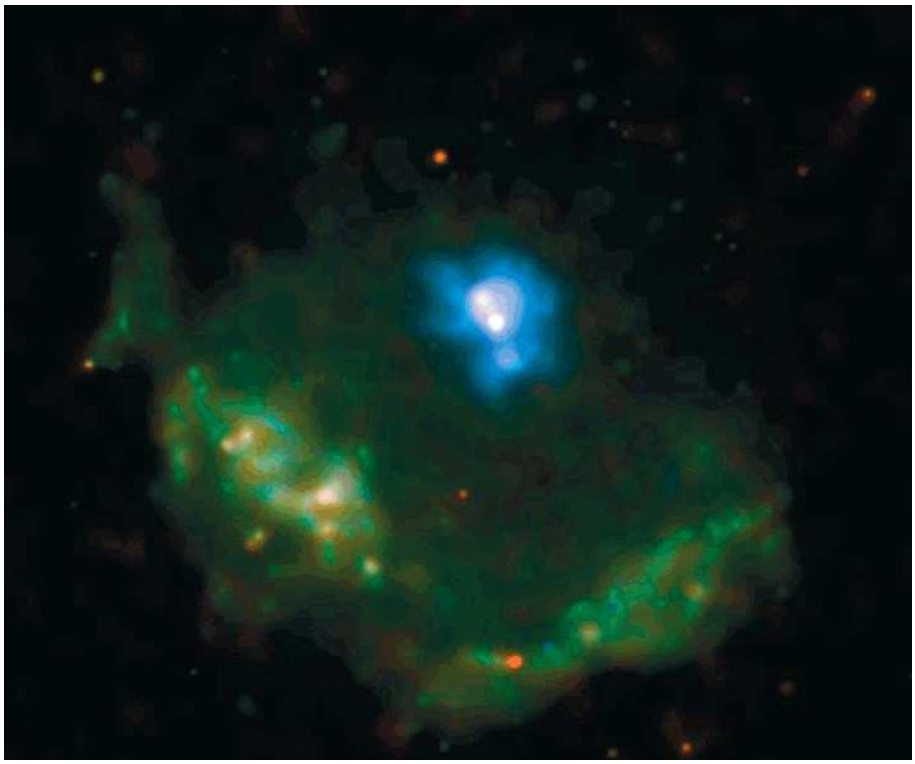

Author:
Ariane Dekker
Study: Physics & Astronomy

Supervisors:
Dr. Lucien Kuiper
SRON
and
Prof. Dr. Cristiane de Morais Smith
Utrecht University

15 June 2016

Abstract

PSR J1846-0258 is a 324 ms pulsar discovered in 1999 at X-ray energies [11]. It is the youngest rotation-powered pulsar known and is located at the centre of SN-remnant Kes 75. The magnetic field strength has a value of $\sim 4.9 \times 10^{13}$ G, which is just above the quantum critical field strength of $B_{cr} = \frac{m_e c^3}{e\hbar} = 4.413 \times 10^{13}$ G. In June 2006 a magnetar-like outburst occurred: a dramatic brightening with spectral softening. It recovered to pre-outburst flux levels at $\frac{1}{e}$-time scale of ~ 55 days [15]. During its outburst, five short magnetar-like bursts (less than $\sim$ 100 ms) were discovered as well as a large timing glitch making phase-coherent timing impossible for a couple of months. Since then, PSR J1846-0258 has been behaving again as a stable rotation-powered pulsar. Deep INTEGRAL and RXTE HEXTE observations showed the detection of pulsed emission up to $\sim$ 150 keV. Its pulsed spectrum mimics that of the canonical soft gamma-ray pulsar PSR B1509-58 [15], but the flux level is about $\sim$ 10 times lower. Therefore, PSR J1846-0258 is an excellent candidate to be detected as a high-energy gamma-ray pulsar (greater than $\sim$ 30 MeV) given the detection of pulsed gamma-rays from PSR B1509-58 up to $\sim$ 300 MeV [16]. For this bachelor thesis I analysed all available Fermi LAT ($>$ 30 MeV) and GBM (8 keV - 2 MeV) data on this pulsar collected over a $\sim$ 7.6 year time period. In this work I discovered for the first time pulsed emission at high-energy gamma-rays in the 30-100 MeV band, while the simultaneously obtained Fermi GBM data made the detection of pulsed soft gamma-ray emission possible up to $\sim$ 300 keV.

Keywords: pulsars: individual: PSR J1846-0258 — gamma-rays: observations

Title page image: Chandra ACIS-S3 combined image of PSR J1846-0258 and its pulsar wind nebula at the centre of supernova remnant Kes 75 divided in the soft (0.5 - 1.15 keV; red), medium (1.15 - 2.3 keV; green) and hard (2.3 - 10.0 keV; blue) energy bands. Source: [18]

Contents

Chapter 1

Introduction

1.1 Evolution towards a neutron star

Stars form in dense cores of molecular clouds in interstellar medium by gravitational collapse. Interstellar gas will then be highly compressed to become a star. Time-scales for a dense molecular cloud core to collapse under its own gravity are around 40 millennia, therefore the galaxy still has clouds that are in hydrostatic equilibrium. When a cloud is disturbed from its stable hydrostatic equilibrium by a pressure wave travelling through the cloud, it has to re-establish the change in pressure. The cloud will collapse if the timespan during the wave travelling from outside to the core is larger than the free-fall time. Conservation of angular momentum will stop the collapse so that a slowly rotating ball of gas is formed with a protostar inside the central region of the disk. The disk contains more angular momentum than a star but because hot gas will move along magnetic field lines, which are rotating along the disk, it will carry angular momentum. This movement forms strong stellar wind. When the protostar is dense and hot enough to ignite Hydrogen fusion it becomes a star. The star fuses Hydrogen to Helium in the core and is now called a main sequence star. The progenitors of the star is mostly determined by its initial mass. Neutron stars have initial mass greater than $\sim 8M_{sun}$ and have short lives as a main sequence star. After the Hydrogen in the core is used up, it keeps on radiating to the colder surrounding. But because there is no Hydrogen left in the core, the Helium core will contract and gravitational energy is converted in thermal energy. Due to the increase in temperature the Hydrogen shell will start fusing into Helium and the star is now a supergiant. Near the end of its lifetime as a star it will have an Iron core with six concentric fusion layers with a Hydrogen-fusing outer shell. The Iron core keeps on growing in size and is supported by degenerate electron pressure. This continues until the core reaches the Chandrasekhar mass, which is the limit of resisting the gravitational collapse through electron degeneracy pressure. The core then starts collapsing and while the density of the core increases, protons and electrons are forming neutrons and neutrinos until the collapse is stopped by neutron degeneracy pressure while the neutrinos escape the sphere. This collapse process is done in 0.1 second and finally a neutron star is formed which has a diameter of around $\sim$ 26 km. Due to the conserved angular momentum during collapse the neutron star is rapidly rotating and highly magnetized, due to magnetic flux conservation. Rapidly rotating and highly magnetized neutron stars are called **pulsars**. [26] These rotating magnetic fields create strong electric fields leading to high voltage differences between surface and magnetosphere. This difference will result in the extraction of electrons from the surface into the magnetosphere. The electrons will be accelerated along magnetic field lines. Electromagnetic radiation is emitted in a beam along the two magnetic axes. This configuration is shown in Figure 1.1.

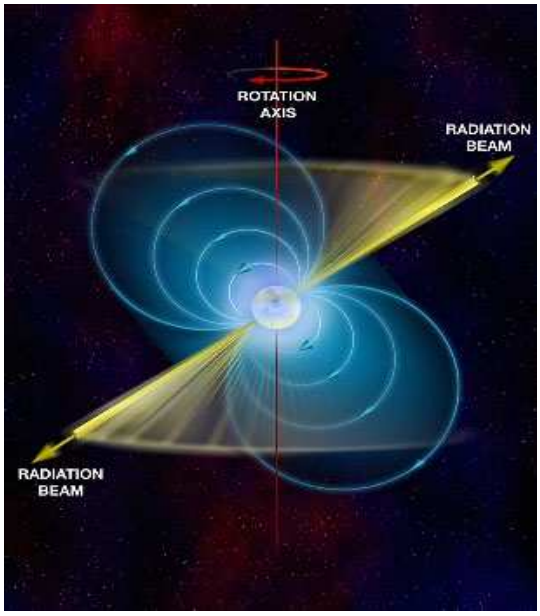

Figure 1.1 – The pulsar has two yellow radiation beams along the magnetic axes which should come within the observer's line of sight to be detected. The blue lines are the magnetic field lines. Source: [13]

Photons transport energy and angular momentum away from the pulsar so that the spin rate is decreasing. Therefore we can characterize a pulsar by the rotational period and the derivative of the rotational period. The energy reservoir that drives the evolution of a pulsar can have different origins. We will concentrate on two relevant subclasses of neutron stars: rotation-powered pulsars and magnetars.

- There are around 2000 **rotation-powered pulsars** known. The energy reservoir is the rotational energy and the emission is powered by the loss of rotational energy, where $\dot{E} = I\omega\dot{\omega}$ [6]. Typical magnetic field strengths are less than $\sim 4 \times 10^{13}$ G.

- At least 10% of newborn neutron stars have sufficiently strong magnetic fields to be called **magnetar**, with fields in excess of $\sim 4 \times 10^{13}$ G. Magnetars can emit sudden enormous amount of gamma-rays which lasts for a few seconds. It's still unknown what's inside the neutron star and there are various theories about the origin of these bursts. One theory is that it would be due to the re-arrangement of the crust. During this process magnetic field lines get strangled and this will release energy [14]. After a burst the pulse period can be irregular for months or years after.

1.2 PSR J1846-0258

I studied PSR J1846-0258, which is a 324 ms pulsar. It is the youngest rotation-powered pulsar known and is located at the centre of supernova remnant Kes 75. Its distance is likely between 5.1 and 7.5 kpc [20], and the pulsar has Galactic coordinates of (l,b)=(29.712015, -0.240245) [12]. Figure 1.2 shows in the 20-70 keV band the Scutum region, which is situated in one of the spirals to the end of the Milky Way's central bar and is rich in star-forming regions. This image was made combining IBIS ISGRI data from INTEGRAL observations totalling 7.35 Ms of exposure time. At the centre of the image, the emission from PSR J1846-0258 and its Pulsar's Wind Nebula (PWN) is visible [15].

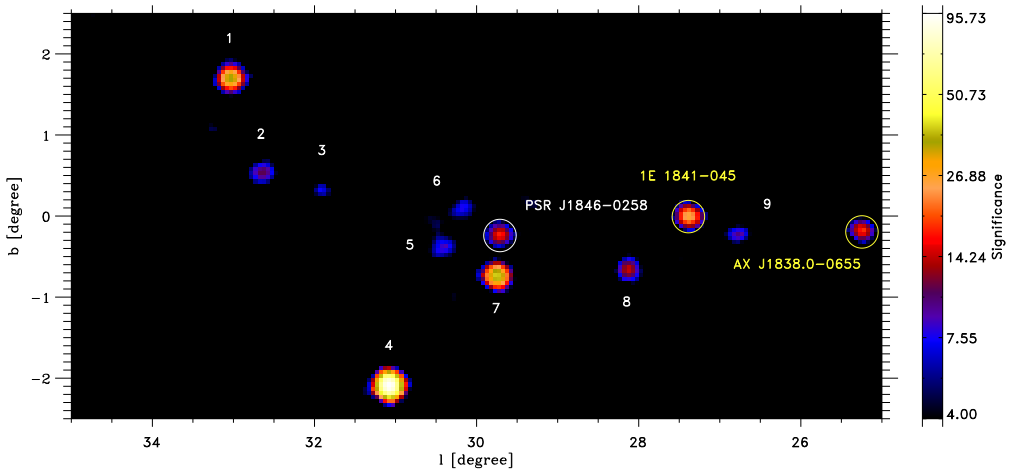

Figure 1.2 – An image of the Scutum region in Galactic coordinates for the 20-70 keV energy range by combining IBIS ISGRI data from INTEGRAL observations totalling 7.35 Ms of exposure time. The white circle indicates PSR J1846-0258 and Kes 75. Source: [15]

The pulsar was discovered in 1999 in a timing analysis of X-ray data from the Rossi X-Ray Timing Explorer (RXTE) and the Advanced Satellite for Cosmology and Astrophysics (ASCA). In previous work [11], pulse profiles were shown using data from RXTE Proportional Counter Array (PCA), RXTE High Energy X-ray Experiment (HEXTE) and INTErnational Gamma-Ray Astrophysics Laboratory (INTEGRAL) Integral Soft Gamma-Ray Imager (ISGRI). The obtained pulse profiles in different energy ranges appear to be energy independent and are shown in Figure 1.3.
PSR J1846-0258 has a magnetic field strength of $\sim 4.9 \times 10^{13}$ G, which is just above the quantum critical field strength of $B_{cr} = \frac{m_e c^3}{e\hbar} = 4.413 \times 10^{13}$ G, implying that quantum electrodynamic physics starts to play a significant role. In June 2006 a magnetar-like outburst occurred: a dramatic radiative brightening accompanied by spectrum softening. The recovery from the pulsed flux increase was modelled as an exponential decay with 1/e time constant of $\sim$ 55 days [10]. During this outburst, five short magnetar-like burst (less than $\sim$ 100 ms) were discovered as well as a large timing glitch making phase-coherence timing impossible for a couple of months. Since then, PSR J1846-0258 has been behaving again as a stable rotation-powered pulsar.

1.3 Research objectives

Due to the increase of exposure of $\sim$ 7.6 years and a new event reconstruction and event selection strategy, Pass 8, we might be able to detect PSR J1846-0258 in the high-energy gamma-ray data. The selection efficiency with the former reconstruction, Pass 7, was not optimal due to residual signals which were induced by background cosmic-rays. The Fermi-LAT collaboration developed an improved reconstruction algorithm to reduce this effect, to better characterize the instrument performance and to improve the angular resolution. Especially below the 100 MeV a huge increase in sensitivity has been reached [19].

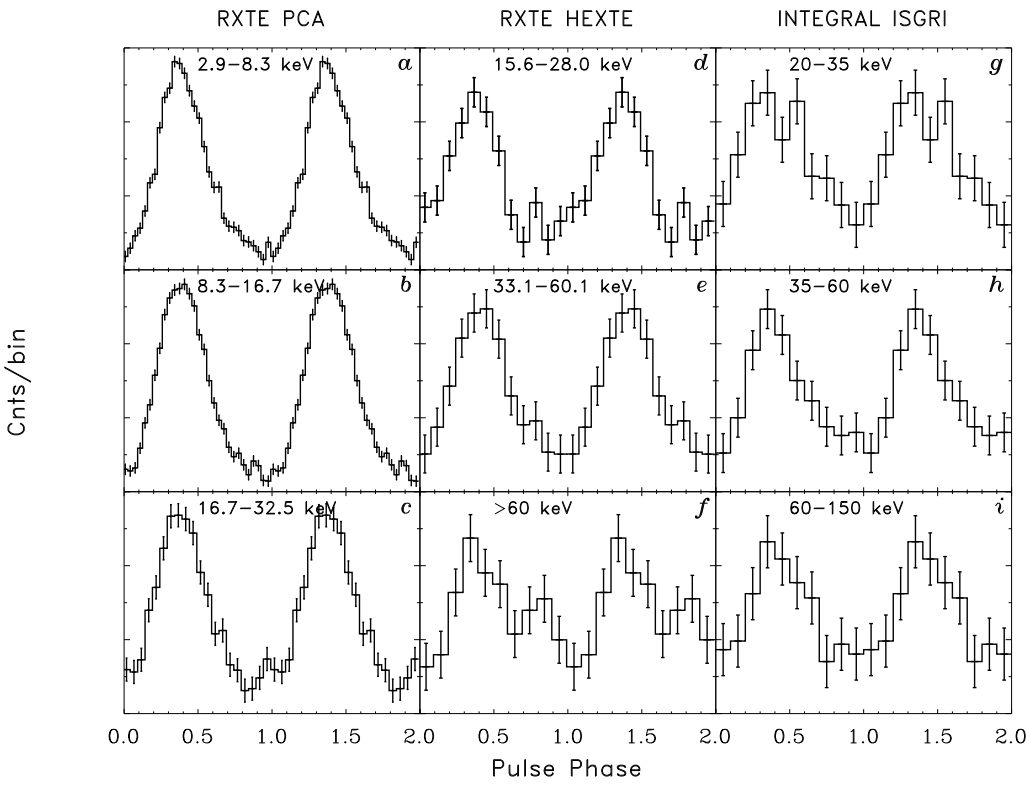

Figure 1.3 – Pulse profile of PSR J1846-0258 using data from RXTE PCA (a-c), HEXTE (d-f) and INTEGRAL ISGRI (g-i) in different energy ranges. Error bars are 1σ on measured counts. Source: [15]

Deep INTEGRAL and RXTE HEXTE observations already showed the detection of pulsed emission up to $\sim$ 150 keV. Its pulsed spectrum mimics that of the canonical soft gamma-ray pulsar PSR B1509-58 [15], but the flux level is around $\sim$ 10 times lower. In Figure 1.4 the energy dependence of the pulsed spectrum of PSR B1509-58 is shown in purple and that of PSR J1846-0258 in green. Due to its similarity in shape and the detection of PSR B1509-58 up to $\sim$ 300 MeV [16], PSR J1846-0258 is an excellent candidate to be detected in high-energy gamma-ray data. For this bachelor thesis I investigated the pulse profile in the high-energy gamma-ray data using the FERMI LAT (above 30 MeV), while FERMI GBM data has been used to explore the soft gamma-ray band (20 keV - 1 MeV).

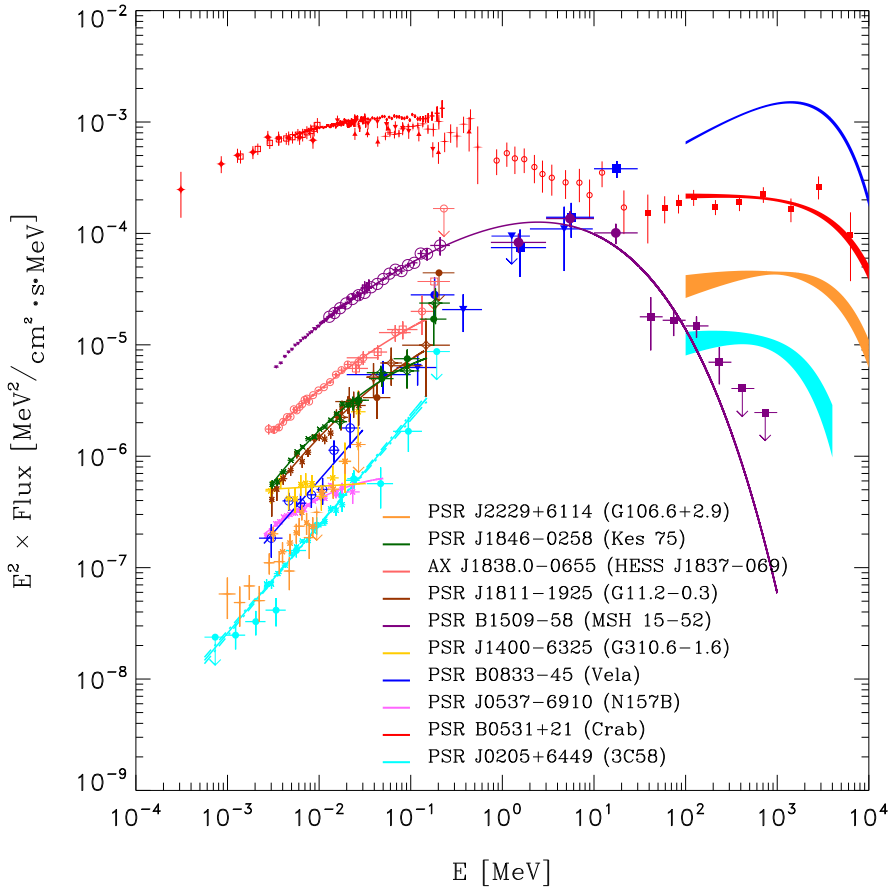

Figure 1.4 – The pulsed spectra of PSR J1846-0258 in green with RXTE and INTEGRAL flux measurements and 1σ error bars. For comparison, soft gamma-ray pulsars like PSR B1509-58 in purple are also included. Source: [16]

Chapter 2

Instrumentation

The Earth's atmosphere is opaque for gamma-rays, therefore I used gamma-ray data from space-borne instruments. For this project I analysed data from Fermi LAT (∼20 MeV - 300 GeV) and GBM (∼8 keV - 40 MeV) using timing models obtained from RXTE PCA and Swift XRT data.

2.1 FERMI

The FERMI Gamma-ray Space Telescope was launched on June 11, 2008 by a Delta 2920H-10 rocket and orbits Earth at approximately 550 km from Earth's surface. The orbital period is 96.5 minutes and the spacecraft performs an all-sky survey. It was designed to have a minimum lifetime of 5 years and a goal of 10 years. The mission consists of three phases where it started with a checkout, then a one year full sky survey and finally at least four years of operations determined by scientific goals and requirements of guest investigations [1] [9].
FERMI contains two instruments to perform gamma-ray observations; the Large Area Telescope (LAT; ∼20 MeV - 300 GeV) and the Gamma-ray Burst Monitor (GBM; ∼8 keV - 40 MeV). They both have a wide field of view (FoV).

2.1.1 LAT

The Large Area Telescope (LAT) is a high-energy gamma-ray telescope covering energy range from 20 MeV to 300 GeV [4]. The LAT measures the directions, energies and arrival times of incident gamma-rays over a FoV of 2.4 steradians and with a timing accuracy of less than 10μs. Incident gamma-rays are converted into electron-positron pairs which are tracked with a precision converter-tracker and calorimeter. A schematic diagram of the LAT is shown in Figure 2.1. The precision converter-tracker tracks the motion of the electron-positron pairs and this information is used to reconstruct the direction of the incident gamma-rays. The calorimeter measures the loss of energy due to the electromagnetic shower resulting from the electron-positron pair and so measures the energy of the incoming gamma-ray photon.

2.1.2 GBM

The Gamma-ray Burst Monitor (GBM) extends the energy range from 8 keV to 40 MeV and is the secondary instrument on the Fermi Gamma-ray Space Telescope. Its objective is to better understand gamma-ray bursts (GRB). GRBs are the most powerful explosions in the universe due to a core collapsing supernova of a massive rotating star or from the merging of neutron star-neutron star / neutron star-black hole. Software on GBM detects and localizes bursts and then transmits data to LAT. The GBM consists of 12 NaI scintillation detectors, two bismuth germanate (BGO) scintillation detectors, a Data Processing Unit (DPU) and a Power Box. The location of the NaI scintillation detectors and BGOs are shown in Figure 2.2.

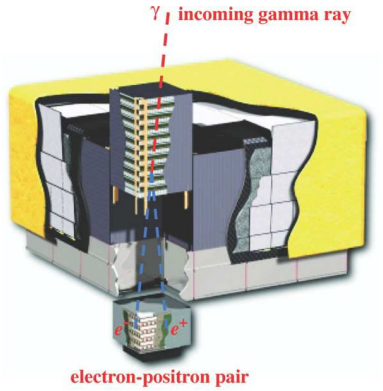

Figure 2.1 – Schematic diagram of the LAT with dimensions of 1.8m x 1.8m x 0.72m. An incoming gamma-ray is converted into an electron-positron pair which is tracked and recorded. Source: [4]

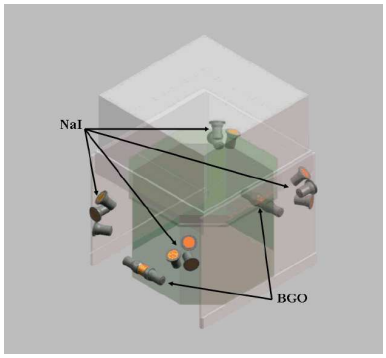

Figure 2.2 – Schematic diagram of the GBM, where the location and orientation of the 12 NaI and the 2 BGO scintillation detectors is shown. Source: [21]

The NaI detectors cover the energy range from 8 keV to 1 MeV and the BGO detectors from $\sim$ 200 keV to $\sim$ 40 MeV. The DPU has three data packets; CTIME (counts are accumulated every 0.256 s in 8 energy channels), CSPEC (counts are accumulated every 4.096 s in 128 energy channels) and TTE (time tagged events during bursts at a timing precision of 2μs in 8 channels). Since November 26, 2011 in nominal operation mode, the GBM is continuously recording to the ground time-tagged events (TTE) with 2μs precision synchronized to GPS [21].

2.2 Swift

Swift was launched in November 20, 2004 by a Delta II 7320-10C. The Swift telescope contains three instruments, which work together to observe Gamma-Ray Bursts (GRBs) and afterglows in the gamma-ray, X-ray, ultraviolet and optical wavebands. Swift discovers around 100 burst per year [27]. The three instruments are the Burst Alert Telescope (BAT) which covers the 15-150 keV range, the X-ray Telescope (XRT) which covers the 0.3-10 keV range and the UV/Optical Telescope (UVOT) which covers the 170-600 nm spectrum. For this bachelor project we made use of the XRT data. The XRT takes images for positioning the source with an higher accuracy. It has several operation modes of which we used the Windowed Timing (WT). The time resolution in the WT mode is 1.7675 ms which is sufficient for making timing models for PSR J1846-0258 (rotational period of 324 ms) [17].

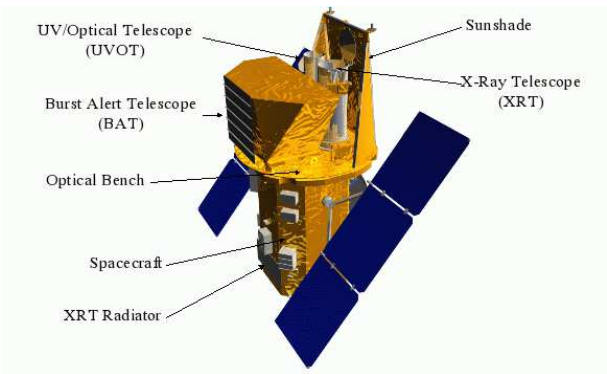

Figure 2.3 – Image of the Swift telescope where you can see the three instruments, covering an energy range of $\sim 0.3 - 150$ keV. Source: [27]

Chapter 3

Data analysis and reduction

In this chapter I describe how events were selected, barycentered and timing models were applied. These timing models have been constructed using Proportional Counter Array (PCA) observations aboard RXTE for the time period June 2008 until December 2011 and Swift X-Ray Telescope (XRT) observations, which included PSR J1846-0258 as of July 2011 in its monitoring program, to continue these timing observations. For every selected event, the arrival time and energy were used for further analysis. For these events, we made pulse-phase distributions and applied statistical methods to derive pulsed emission significances.

3.1 Event selection FERMI

The instruments aboard FERMI detect a high level of background radiation. The following selection has been applied to both FERMI instruments.

- Fermi will be in the South Atlantic Anomaly (SAA) for 15% of its time [9]. This is an area of the Van Allen radiation belts where charged particles from solar winds are being trapped. These belts are aligned with the magnetic axis of the Earth. The high density of charged particles can be problematic for the operation of the spacecraft, therefore the instruments are switched of while passing the SAA.

3.1.1 Event selection and data reduction FERMI GBM

The Earth's atmosphere is a strong background source of gamma-ray radiation. Therefore we applied a so-called Earth's zenith cut by selecting only those observation periods in which the angle between the detector pointings and Earth's zenith angle is less than 128°. The latter value was obtained through optimalisation studies using X-ray binary Her X-1 [5].
We also made a selection on the angle between the detector pointing and the source direction, and allowed only angles less than 58°. This value was also derived from optimalisation studies using Her X-1.
In the FoV there can occur activities originating from other sources and therefore obvious short duration bursts are excluded.
To study the 324 ms pulsar PSR J1846-0258, GBM TTE data has been used offering a 2μs time resolution for 128 spectral channels. Data taking in TTE-mode has become the default since November 26, 2012. To speed up the data processing, particularly the barycentering process, we degrade the sampling time bin-size to 10 ms, which is still amply sufficient for the timing analysis.

3.1.2 Event selection and data reduction FERMI LAT

Event and spacecraft data were downloaded from the Fermi Science Support Centre of NASA covering the period August 4, 2008 until March 11, 2016. Converting to MJD this corresponds to the time period between MJD 54559 and MJD 57458. We selected only events within angular distance less than 12° from the source direction. For this angular selection, we allowed only a certain fraction of the incident gamma-rays. An energy dependent cone is applied so that 68% of source photons is accepted.
We made use of the tool gtselect, provided by the NASA Fermi Science Support Center, to make further cuts in the event data file. The source class event parameter was set to only include events with a high probability of being celestial photons. The incoming angle between the event direction and the Earth's zenith was set to maximal 105°. [9]

3.2 Barycentering

The spacecraft and Earth are continuously moving through the non-inertial solar system. Therefore we will convert the arrival times of the selected events to a fictitious observer located at the solar system barycentre, which is the best conceivable inertial system. To perform this barycentering, various travel time delays and some relativistic effects have to be taken into account. Required in this process are:

- The instantaneous spacecraft position with respect to the Earth's centrer.
- The source location on the sky where we used the right ascension and declination (α, δ)=$(18^h46^m24^s.94, -02^o58'30".1)$ for epoch J2000, or in Galactic coordinates (l,b)=$(29.7120125, -0.240245)$. [12]
- The JPL Solar System ephemeris DE200, which provides the positions and velocities of the Sun, Earth, moon and planets (and major asteroids) as a function of time.

For FERMI LAT data I used the tool gtbary, provided by the NASA Fermi Science Support Centre, where barycentric corrections are made to photon arrival times, while for the FERMI GBM data I used IDL tools developed by SRON.

3.3 Timing analysis

Timing models, ephemerides, describe the rotational behaviour of the pulsar as a function of time and includes the frequency and the first and second derivative of the frequency. RXTE has been monitoring PSR J1846-0258 for 13 years. From July 2011 Swift XRT started monitoring PSR J1846-0258 in anticipation of the decommissioning of RXTE in early 2012.
We covered the period from MJD 54559 (August 4, 2008) up to MJD 57458 (March 11, 2016). Table 3.1 shows the timing models, RXTE PCA and Swift XRT based, used in this project. The ephemerides derived from RXTE PCA data are listed as entries 1 to 5. Entries 6-8 are new timing models based on Swift monitoring data. To obtain these timing models, given the low signal-to-noise of these Swift XRT observations, is rather difficult and complicated. Therefore, before applying these models on FERMI LAT data, we wanted to verify its validity using independent datasets. For this purpose we used FERMI GBM data. The 8 ephemerides shown in Table 3.1 are the ones we used for FERMI LAT and GBM data. Due to the loss of phase coherence between MJD 56185 and MJD 56338 we have a gap between entry 6 and 7. In total we covered 2.3×10^8 seconds of data, which corresponds to ~ 8 years.

Table 3.1 – Phase-coherent ephemerides derived from RXTE PCA and Swift XRT data

Entry	Start [MJD]	End [MJD]	t_0, Epoch [MJD]	ν [Hz]	$\dot{\nu}$ $\times 10^{-11}$ [Hz/s]	$\ddot{\nu}$ $\times 10^{-21}$ [Hz/s^2]
1	54559	55070	54559	3.0637028069105	-6.67156	3.13
2	55056	55175	55056	3.0608408932423	-6.66505	12.3
3	55154	55348	55222	3.0598859484927	-6.65645	1.83
4	55348	55541	55494	3.0583227179115	-6.64875	2.54
5	55488	55906	55811	3.0565029361132	-6.63946	3.58
6	55588	56185	55811	3.0565029362756	-6.63941	3.67
7	56338	56966	56652	3.0516882592209	-6.61345	3.28
8	56940	57458	57199	3.0485662050460	-6.59866	3.13

In Figure 3.1 the pulse frequency evolution from detection of PSR J1846-0258 in April 18-21, 1999 till March 11, 2016 relative to the pre-outburst timing model is shown. Former work explored the period from January 30, 2000 to November 7, 2007 [15]. The magnetar-like outburst of 2006 is clearly visible around MJD 54000, where data points are plotted with 1σ error bars. The lines show phase coherent timing models. The time span we covered in this work from MJD 54782 to MJD 57459 is shown, using the ephemerides of Table 3.1 with the time gap between MJD 56185 and MJD 56338.
The vertical solid line is when FERMI was launched, the dot-dashed line is when RXTE was decommissioned and the dashed line is when the GBM TTE mode started. Shaded vertical bars indicate observation gaps due to solar/moon constraints.

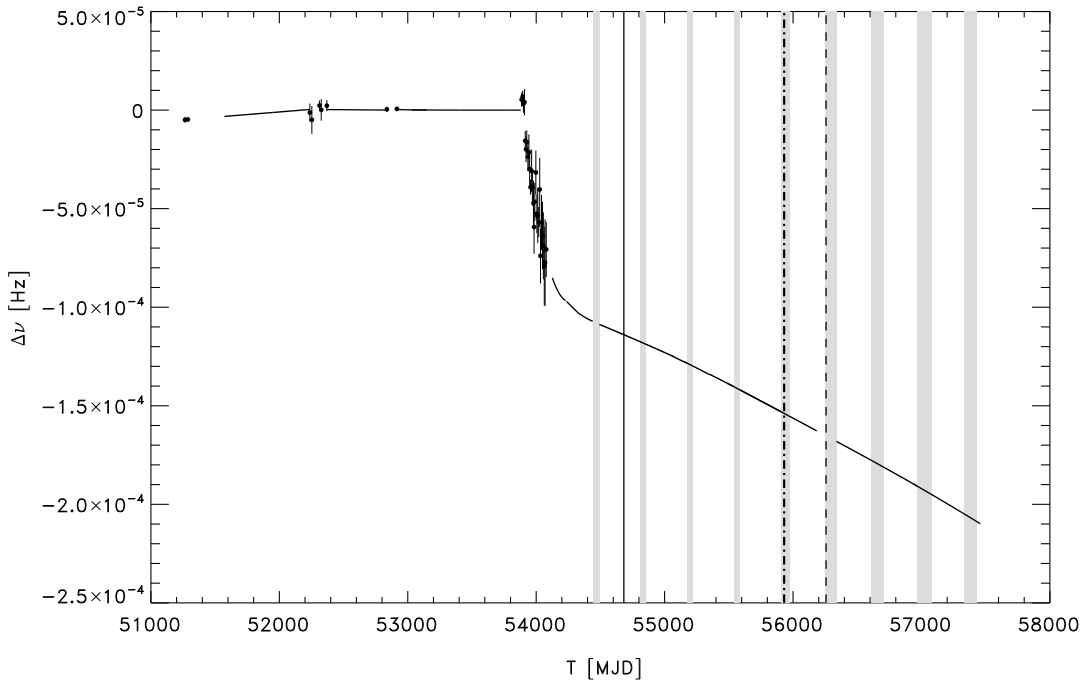

Figure 3.1 – The rotational behaviour of PSR J1846-0258 from the discovery in 1999 to March 11, 2016. In this work we covered the period from August 4, 2008 to March 11, 2016 with a gap from September 15, 2012 to February 15, 2013 due to the loss of phase coherence.

We first calculated the pulse phase, ϕ , of an event with barycentric arrival time t, which is done using a Taylor series:

$$\phi(t) = \phi(t_0) + \nu(t - t_0) + \frac{1}{2}\dot{\nu}(t - t_0)^2 + \frac{1}{6}\ddot{\nu}(t - t_0)^3 + ..., \tag{3.3.1}$$

where ν is the pulsar's frequency, $\dot{\nu}$ the first derivative of the frequency, $\ddot{\nu}$ the second derivative of the frequency and t_0 the epoch. These phases are sorted in a pulse-phase histogram, called pulse profile, across phase [0,1].

In this thesis we used a Z_n^2-test to derive pulsed emission significances, which uses the same principle as Fourier analysis. The Z_n^2-test is distributed as a chi-squared with 2n degrees of freedom for large samples and provides a measure for the signal-to-noise ratio of the pulsed emission. The statistical variable Z_n^2 is defined as:

$$Z_n^2 = \frac{2}{N}\sum_{k=1}^{n}[(\sum_{i=1}^{N} cosk\phi_i)^2 + (\sum_{i=1}^{N} sink\phi_i)^2], \tag{3.3.2}$$

where N is the number of events and n the number of harmonics [6].

Chapter 4

Results and discussion

4.1 GBM

I folded the barycentered event times of the selected GBM events (128 spectral channels) collected during mission weeks 246-404 (i.e. from February 14, 2013 to March 2, 2016; MJD 56337 to MJD 57449) on the timing models shown in Table 3.1. The mean exposure time per NaI detector was 16.86 ms. This resulted in a pulse-phase distribution for the 20-300 keV band, that deviates from uniformity at a 6.2σ level applying a Z_1^2-test (see section 3.3 and also Figure 4.3b). The 6.2σ for the 20-300 keV profile demonstrates that the timing models obtained using Swift XRT WT data are appropriate because it reconstructs the shape and alignment of the 'known' 20-150 keV INTEGRAL ISGRI/RXTE HEXTE profiles, and thus these Swift timing models can also be applied to the simultaneously obtained FERMI LAT data.
A break-down of the GBM data yielded for the 20-100 keV bands significances of 5.2σ, 3.2σ and $< 3\sigma$ respectively. The corresponding profiles are shown in Figure 4.1, where the number of counts/bin is plotted against the phase with 1σ error bars. This demonstrates that we detected PSR J1846-0258 for the first time above 100 keV.

4.2 LAT

Phase folding FERMI LAT data and applying a Z_1^2-test resulted in a deviation of 3.7σ in the 30-100 MeV energy range. The obtained pulse profile can be seen in Figure 4.2a where the number of counts/bin is plotted against the phase. We see the pulse peak at the expected phase, while in Figure 4.2b (at energies > 100 MeV) we cannot distinguish the pulse any more from the background. Figure 4.3c shows the 30-100 MeV pulse profile again, now with superposed best fit to the shape of the 20-150 keV INTEGRAL ISGRI profile (see [15] Figure 3). We can restrict further the energy dependent cone to include 85% of the 68% acceptance cone, then even a significance of 4.4σ is reached.

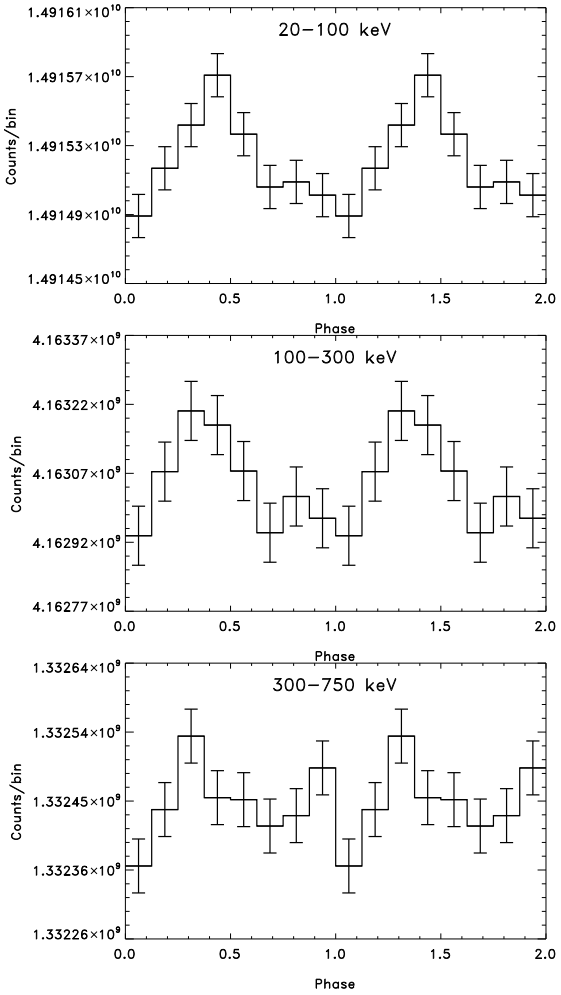

Figure 4.1 – Collage of pulse profile of PSR J1846-0258 using GBM data from February 14, 2013 to March 4, 2016 with the following energy ranges: a) 20-100 keV b) 100-300 keV c) 300-750 keV. Error bars are 1σ.

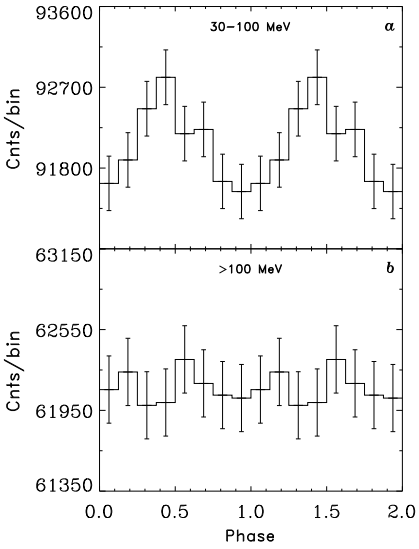

Figure 4.2 – Collage of pulse profile of PSR J1846-0258 using LAT data from August 4, 2008 to March 11, 2016 with the following energy ranges: a) 30-100 MeV b) above 100 MeV. Error bars are 1σ.

4.3 Swift XRT, FERMI GBM / LAT collage

Making use of the timing models as listed in Table 3.1 we can compare the pulse-profiles across a broad energy band, from soft X-rays up to high-energy gamma-rays. This is shown in Figure 4.3 with in the top panel the Swift XRT 2.5-10 keV profile, in the middle the FERMI GBM 20-300 keV profile and in the bottom panel the FERMI LAT 30-100 MeV profile. The best INTEGRAL ISGRI 20-150 keV shape fit is superposed, demonstrating the proper alignment across many years of data taken.

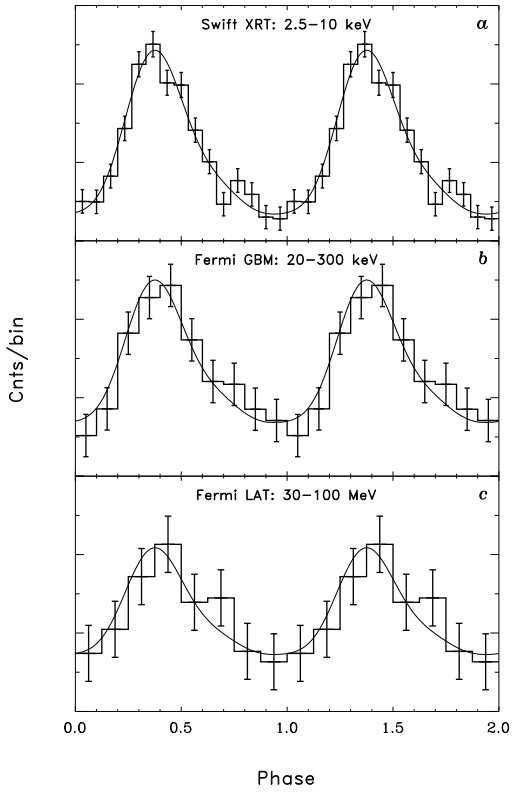

Figure 4.3 – Pulse profile of PSR J1846-0258 using data from a) Swift XRT (2.5-10 keV), b) Fermi GBM (20-300 keV) and c) Fermi LAT (30-100 MeV) with 1σ error bars.

Chapter 5

Summary and future research

In this bachelor's research project I detected pulsed gamma-ray emission up to 100 MeV from high B-field pulsar PSR J1846-0258 for the first time. This was possible by using the long FERMI LAT exposure time ($\sim$ 7.6 years) on the source, the updated event reconstruction algorithm (Pass 8) for FERMI LAT, yielding significantly improved sensitivity at low-energy gamma-rays, and accurate phase-coherent timing models. In the soft gamma-ray band improved pulse-phase distributions, especially for the 100-300 keV band, has been obtained by phase-folding FERMI GBM data.
These results are issued as an astronomical telegram (ATEL) #9077 on May 24, 2016 (see Figure 5.1).
Increasing the FERMI LAT/GBM exposure time with a couple of years will result in better constrained high-energy pulsar characteristics, provided that the Swift XRT monitoring continues for a couple of years more. In particular, improved spectral information is envisioned.

The Astronomer's Telegram
Post | Search | Policies
Credential | Feeds | Email

26 May 2016; 11:22 UT

[Previous | Next]

The Fermi LAT/GBM detection of pulsed gamma-ray emission from PSR J1846-0258 up to 100 MeV

ATel #9077; *Lucien Kuiper (SRON), Ariane Dekker (SRON, UU)*
on 24 May 2016; 13:57 UT
Credential Certification: Lucien Kuiper (L.M.Kuiper@sron.nl)

Subjects: X-ray, Gamma Ray, Neutron Star, Pulsar

Applying phase coherent timing models, created using RXTE PCA and Swift XRT monitoring data of PSR J1846-0258 covering the period August 4, 2008 - March 11, 2016 (MJD 54682 - 57458), in timing analyses of Fermi LAT (PASS8) and Fermi GBM (TTE) data yielded for the first time the detection of pulsed gamma-ray emission from PSR J1846-0258 up to 100 MeV.

Phase folding the barycentered Fermi LAT events (period MJD 56185-56338, i.e. Sept. 15, 2012 - Feb. 15, 2013 has been excluded because of the loss of phase coherence), falling within the energy dependent 68%-cone, resulted in a 30-100 MeV pulse profile, which deviates more than 3.7 sigma (single trial) from uniformity applying a Z_1^2-test with its single -slightly asymmetric- pulse aligned with the Swift XRT 2.5-10 keV profile (note: a slightly tighter cone selection of 85% of the 68%-cone yielded a 4.4 sigma signal). For energies above 100 MeV no significant pulsed emission has been detected indicating the softness of the spectrum at these energies. Assuming a similar spectral shape for the pulsed spectrum as the 'canonical' soft gamma-ray pulsar PSR B1509-58 (see Kuiper & Hermsen 2015; MNRAS 449, p. 3839) the measured 30-100 MeV pulsed count rates for PSR J1846-0258 and PSR B1509-58 translate in a 30-100 MeV pulsed flux of (1.41+/- 0.43)E-11 erg/cm^{2}s for PSR J1846-0258, about 4-5 times weaker than that observed for PSR B1509-58.

We also phase-folded the time-tagged events (TTE - the default operation mode since Nov. 26, 2012; 2 us precision; 128 spectral channels) from the 12 NaI (8-2000 keV) detectors of the Fermi GBM collected during Fermi mission weeks 246-404 (i.e.from Feb. 14, 2013 - March 2, 2016). We detected pulsed emission at 6.2 sigma confidence for the 20-300 keV band, applying a Z_1^2-test, with the single asymmetric profile aligned with the 2.5-10 keV Swift XRT profile. For the bands 20-100 keV and 100-300 keV we found 5.2 sigma and 3.2 sigma, respectively. The mean (screened) exposure per NaI detector was 16.86 Ms. A pulse profile collage showing the contemporaneous Swift XRT (2.5-10 keV), Fermi GBM (20-300 keV) and Fermi LAT (30-100 MeV) profiles with superposed the best fit RXTE PCA 2-20 keV pulsed profile is shown at PSR J1846-0258 profile .

Our results confirm that the shape of the pulsed spectrum of PSR J1846-0258 mimics that of PSR B1509-58, and that its spectrum extends now up to 100 MeV. Future Fermi observations of PSR J1846-0258, assuming a continuation of the Swift XRT monitoring program of PSR J1846-0258, will improve the knowledge of the soft gamma-ray spectral characteristics considerably. We acknowledge the use of public Fermi GBM and LAT as well as Swift XRT data.

[Telegram Index]

Figure 5.1 – Telegram on astronomerstelegram.org, #9077 on May 24, 2016.

Chapter 6

Acknowledgement

The bachelor research project at SRON was an enjoyable and inspiring experience. It has given me an insight of doing research within astrophysics. SRON gave me the opportunity to attend the NAC (Netherlands Astronomy Conference), which I am very thankful for. I would like to thank my daily supervisor dr. Lucien Kuiper for assisting me in the right direction, his availability and opportunity to do this research project. Also I would like to thank prof. Dr. Cristiane de Morais Smith for making this project possible by being my supervisor.

Bibliography

[1] A. A. Abdo et al. “Fermi/large area telescope bright gamma-ray source list”. In: *The Astrophysical Journal Supplement Series* 183.1 (2009), p. 46.

[2] A. A Abdo et al. “The second Fermi Large Area Telescope catalog of gamma-ray pulsars”. In: *The Astrophysical Journal Supplement Series* 208.2 (2013), p. 17.

[3] R. F. Archibald et al. “On the braking index of the unusual high-B rotation-powered pulsar PSR J1846-0258”. In: *The Astrophysical Journal* 810.1 (2015), p. 67.

[4] W. B. Atwood et al. “The Large Area Telescope on the Fermi gamma-ray space telescope mission”. In: *The Astrophysical Journal* 697.2 (2009), p. 1071.

[5] Felix ter Beek. “FERMI GBM detections of four AXPs at soft gamma-rays”. An optional note. MA thesis. University of Amsterdam, 2012.

[6] R. Buccheri et al. “Search for short bursts of gamma-ray emission in spark chamber data: application to COS-B”. In: *Astronomy and Astrophysics* 277 (1993).

[7] D. J. Champion et al. “Measuring the mass of solar system planets using pulsar timing”. In: *The Astrophysical Journal Letters* 720.2 (2010), p. L201.

[8] “Course of National Radio Astronomy Observatory”. In: *http://www.cv.nrao.edu/course/astr534/PulsarTiming.html* (accessed June 2016).

[9] “Fermi Science Support Center”. In: *http://fermi.gsfc.nasa.gov/ssc/* (accessed June 2016).

[10] Fotis P Gavriil et al. “Magnetar-like emission from the young pulsar in Kes 75”. In: *Science* 319.5871 (2008), pp. 1802–1805.

[11] E. V. Gotthelf et al. “A 700 year-old pulsar in the supernova remnant kesteven 75”. In: *Astrophysical Journal* 542 (2000).

[12] David J Helfand, Benjamin F Collins, and EV Gotthelf. “Chandra X-ray imaging spectroscopy of the young supernova remnant Kesteven 75”. In: *The Astrophysical Journal* 582.2 (2003), p. 783.

[13] “Illustration of a pulsar with rotation axis and radiation beams”. In: *http://www.projectrho.com/public$_h$tml/rocket/astrodeck.php* (accessed June 2016).

[14] C. Kouveliotou, R. C. Duncan, and C. Thompson. “Magnetars”. In: *Scientific American* 288.2 (2003), pp. 34–41.

[15] L. Kuiper and W. Hermsen. “High-energy characteristics of the schizophrenic pulsar PSR J1846-0258 in Kes 75”. In: *Astronomy and Astrophysics* 501 (2009).

[16] L Kuiper and W Hermsen. “The soft γ-ray pulsar population: a high-energy overview”. In: *Monthly Notices of the Royal Astronomical Society* 449.4 (2015), pp. 3827–3866.

[17] L Kuiper et al. “Temporal and Spectral Evolution in X-and γ-Rays of Magnetar 1E 1547.0–5408 since its 2008 October Outburst: The Discovery of a Transient Hard Pulsed Component after its 2009 January Outburst”. In: *The Astrophysical Journal* 748.2 (2012), p. 133.

[18] Harsha Sanjeev Kumar and Samar Safi-Harb. “Variability of the High Magnetic Field X-Ray Pulsar PSR J1846–0258 Associated with the Supernova Remnant Kes 75 as Revealed by the Chandra X-Ray Observatory”. In: *The Astrophysical Journal Letters* 678.1 (2008), p. L43.

[19] H. Laffon and D. A. Smith. "New pulsars detected in gamma-rays with the Fermi-LAT". In: 5th Fermi Symposium. 2014.

[20] Denis A Leahy and WW Tian. "The distance of the SNR Kes 75 and PWN PSR J1846-0258 system". In: *Astronomy & Astrophysics* 480.2 (2008), pp. L25–L28.

[21] C. Meegan et al. "The Fermi gamma-ray burst monitor". In: *The Astrophysical Journal* 702.1 (2009), p. 791.

[22] W. A. Mulder and R. E. Plessix. "How to choose a subset of frequencies in frequency-domain finite-difference migration". In: *Geophysical Journal International* 158.3 (2004), pp. 801–812.

[23] "NASA's high energy astrophysics science archive research center". In: *https://heasarc.gsfc.nasa.gov/docs/xte/abc/time_tutorial.html* (accessed June 2016).

[24] D. Parent et al. "Observations of Energetic High Magnetic Field Pulsars with the Fermi Large Area Telescope". In: *The Astrophysical Journal* 743.2 (2011), p. 170.

[25] S. G. Ryan and A. J. Norton. *Stellar evolution and nucleosynthesis*. pp. 163-169. 2010.

[26] B. Ryden and B. M. Peterson. *Foundation of Astrophysics*. pp. 393-431. 2011.

[27] "The Swift gamma-ray burst mission". In: *http://swift.gsfc.nasa.gov/* (accessed June 2016).